PHYSICAL REVIEW A **95**, 013404 (2017)

Spin-orbit delays in photoemission

I. Jordan,[1] M. Huppert,[1] S. Pabst,[2,3] A. S. Kheifets,[4] D. Baykusheva,[1] and H. J. Wörner[1,*]
[1]*Laboratorium für Physikalische Chemie, ETH Zürich, Vladimir-Prelog-Weg 2, CH-8093 Zürich, Switzerland*
[2]*Center for Free-Electron Laser Science, DESY, Notkestrasse 85, D-22607 Hamburg, Germany*
[3]*ITAMP, Harvard-Smithsonian Center for Astrophysics, 60 Garden Street, Cambridge, Massachusetts 02138, USA*
[4]*Research School of Physical Sciences, The Australian National University, Canberra ACT 0200, Australia*
(Received 12 July 2016; published 10 January 2017)

Attosecond delays between photoelectron wave packets emitted from different electronic shells are now well established. Is there any delay between electrons originating from the same electronic shell but leaving the cation in different fine-structure states? This question is relevant for all attosecond photoemission studies involving heavy elements, be it atoms, molecules or solids. We answer this fundamental question by measuring energy-dependent delays between photoelectron wave packets associated with the $^2P_{3/2}$ and $^2P_{1/2}$ components of the electronic ground states of Xe^+ and Kr^+. We observe delays reaching up to 33 ± 6 as in the case of Xe. Our results are compared with two state-of-the-art theories. Whereas both theories quantitatively agree with the results obtained for Kr, neither of them fully reproduces the experimental results in Xe. Performing delay measurements very close to the ionization thresholds, we compare the agreement of several analytical formulas for the continuum-continuum delays with experimental data. Our results show an important influence of spin-orbit coupling on attosecond photoionization delays, highlight the requirement for additional theory development, and offer a precision benchmark for such work.

DOI: 10.1103/PhysRevA.95.013404

I. INTRODUCTION

In recent years, the measurement and interpretation of delays in photoemission has become one of the most active areas within attosecond science. All efforts have so far concentrated on delays between photoelectron wave packets originating from different electronic shells of atoms [1,2], solids [3–5], and molecules [6] (see Ref. [7] for a review). These studies have revealed temporal delays of a few tens of attoseconds between photoelectrons associated with different final *electronic* states of the cation.

In this article, we add an additional dimension to this field of research by addressing the role of atomic fine structure on attosecond photoemission delays. This progress is made possible by a considerably improved energy resolution in conjunction with advanced data-acquisition techniques. We measure the temporal delay between photoelectron wave packets associated with different final *spin-orbit* states of the electronic ground states of Kr^+ and Xe^+. Whereas the delays are very small ($\leqslant$8 as) in Kr, much larger delays up to 33 ± 6 as are measured in the case of Xe. These results show that atomic fine-structure effects are not, in general, negligible compared to electronic effects. We expect this result to extend from atoms, over molecules to solids and to be particularly important for heavy elements, since spin-orbit coupling scales with nuclear charge to the fourth power. We further show that our results point to significant shortcomings in state-of-the-art theories. A detailed consideration of the possible origins of these discrepancies leads us to identify an incomplete description of electron correlation as the most likely origin. Our results further offer an approach to investigating spin-orbit coupling, which is a ubiquitous phenomenon with a wide range of implications in physics and chemistry. For example, spin-orbit coupling is responsible for the creation of spin-polarized electrons in the photoionization of atoms and solids [8,9] and for intersystem crossing in molecules, the importance of which has been underestimated for a long time, particularly in molecules containing relatively light elements [10].

We compare our results with two of the most accurate currently available *ab initio* theories, i.e., the time-dependent configuration-interaction singles (TDCIS) theory and the relativistic random-phase approximation (RRPA). The TDCIS theory is an explicitly time-dependent multielectron method that we use to directly simulate our experiment, without additional approximations. The RRPA represents the state of the art in atomic photoionization, particularly of heavy elements, achieving near-quantitative agreement with photoionization cross sections and angular distributions [11,12]. The RRPA is a time-independent method that we couple with an analytical treatment of the continuum-continuum transitions to describe our experiments based on attosecond interferometry [13].

Our work addresses the topic of the fine-structure dependence of photoemission delays. This dependence provides access to the manifestation of relativistic effects in photoionization delays. It therefore represents a testing ground for theory that we exploit in two complementary ways. First, by performing measurements at high photon energies ($\geqslant$25 eV), where the contributions of the Coulomb singularity and the differences of the continuum-continuum delays between the closely spaced spin-orbit levels are both negligible, our measurements probe the influence of doubly excited states and the effect of relativistic phase shifts between the photoelectron continua accessed at the one-photon level. These phase shifts have never been measured before because they are inaccessible to static photoelectron measurements, which are only sensitive to phase shifts between continua belonging to the same ionization threshold. Our experimental results are in significant disagreement with theory, demonstrating the need for further development. Second, performing measurements

*Corresponding author: hwoerner@ethz.ch; www.atto.ethz.ch

in the vicinity of the ionization threshold, where the different ionization potentials of the two spin-orbit states completely dominate over the relativistic effects on the delays, we test the performance of several analytical formulas for the continuum-continuum transitions derived for the hydrogen atom in describing experimental data for heavier atoms.

II. EXPERIMENTS

The experimental setup consists of an actively stabilized attosecond beamline [14] and a magnetic-bottle photoelectron spectrometer [15]. The photoelectron resolution is sufficient to fully resolve the spin-orbit splittings of Kr^+ (0.66 eV) and Xe^+ (1.31 eV) beyond the highest kinetic energies reported in this work. High-harmonic generation in a gas cell filled with 10 mbar argon is driven by a 1.5 mJ, 30-fs laser pulse centered at 800 nm. These laser pulses are generated by an amplified titanium:sapphire laser system (Femtopower Pro V CEP by Femtolasers). The generated attosecond extreme-ultraviolet (XUV) pulse train is separated from the residual infrared (IR) pulse under vacuum by means of a perforated off-axis parabolic mirror that simultaneously recollimates the IR beam. The XUV beam is refocused by a toroidal mirror and is recombined with the IR beam by means of a second perforated off-axis parabolic mirror. The delay between XUV and IR is varied by tuning the length of the IR beam path and is actively stabilized during the measurement to a residual jitter of ∼30 as [14]. We note that this jitter does not affect the accuracy of the measured delays, because we measure relative delays. Photoelectrons generated from the overlapping XUV and IR pulses are collected and energy analyzed using a ∼0.9-m-long magnetic-bottle spectrometer equipped with a permanent magnet. Electron time-of-flight spectra are acquired on a single-shot basis using a digitizer card (Agilent U1071A). A chopper wheel is used in the IR beam path to block every other laser shot and to record two-color (XUV and IR) and one-color (XUV-only) spectra in immediate temporal sequence. This approach substantially improves the signal-to-noise ratio and generates high-fidelity difference spectrograms that are used in the subsequent analysis.

III. EXPERIMENTAL RESULTS

Figure 1 illustrates the experimental results and data analysis. Large positive delays correspond to the XUV pulse train preceding the IR pulse. In the case of Kr (a) all photoelectron lines and side bands are fully resolved. The relative phases of the side-band oscillations $\phi^q_{3/2} - \phi^q_{1/2}$, for a given side-band order q, were determined by averaging the complex-valued Fourier transform of the difference spectrogram over the width of the side bands and the width of the oscillation frequency in the Fourier domain. The proximity of the IR-photon energy (1.55 eV) to the spin-orbit splitting in the ^2P ground state of Xe^+ (1.31 eV) causes partial overlap between the $^2P_{3/2}$ sideband of a given order and the $^2P_{1/2}$ photoelectron signal generated by the next-higher harmonic order [see Fig. 1(b)]. We overcome this challenge by analyzing the difference spectrogram (XUV+IR minus XUV-only), acquired on a single-shot basis, with a two-dimensional fitting procedure using common oscillation frequencies. The two sidebands of the same harmonic order, and the two high-harmonic peaks with which they partially overlap, are analyzed simultaneously to extract the measured phase difference $\phi^q_{3/2} - \phi^q_{1/2}$. The success of this data-analysis approach is demonstrated by the weakness of periodic structures in the residuals. This analysis strategy will be particularly useful to perform attosecond interferometry on systems with complex photoelectron spectra [6].

Figure 2 shows the measured spin-orbit delays $\Delta\tau^q = (\phi^q_{3/2} - \phi^q_{1/2})/(2\omega)$, where ω is the IR-laser angular frequency, between photoelectron wave packets associated with the $^2P_{3/2}$ and $^2P_{1/2}$ spin-orbit components of the electronic ground states of Kr^+ and Xe^+. In the case of Kr, all delays are smaller than 8 attoseconds in magnitude. In the case of Xe, the measured delays are larger, reaching from -9 ± 4 as at 21.7 eV to $+33 \pm 6$ as at 33.4 eV. All error bars represent 95%

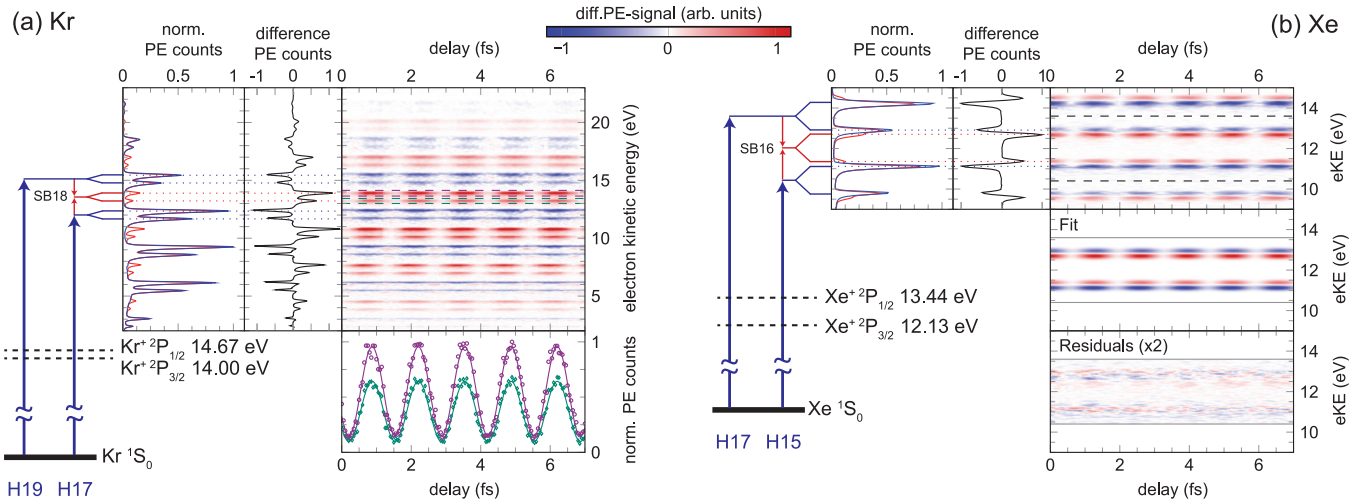

FIG. 1. Measurement of delays between photoelectron wave packets associated with the $^2P_{3/2}$ and $^2P_{1/2}$ final states of Kr^+ and Xe^+. An attosecond pulse train consisting of H11–H27, superimposed with an IR pulse centered at 800 nm is used to ionize the neutral atoms. Photoelectron spectra are acquired in the presence and absence of the IR field and subtracted on a single-shot basis. In the case of Xe, the two-dimensional fitting procedure of the difference spectrograms is illustrated.

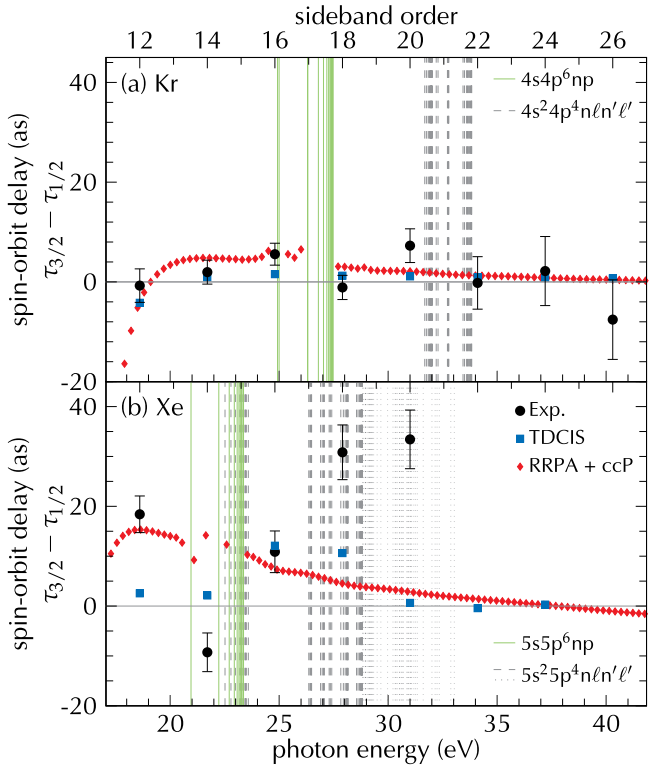

FIG. 2. Delays ($\tau^{\rm tot}_{3/2} - \tau^{\rm tot}_{1/2}$) between photoelectrons associated with the $^2P_{3/2}$ and $^2P_{1/2}$ final states of (a) Kr^+ and (b) Xe^+. The experimental results (circles with error bars) are compared to TDCIS calculations (squares) and RRPA calculations with added continuum-continuum contribution according to Eq. (3) (diamonds). The green (full) lines represent singly excited states, whereas the gray (dashed or dotted) lines represent doubly excited states given in Ref. [16]. The dashed gray lines represent states assigned to specific series and the dotted lines in panel (b) unassigned states.

confidence intervals based on 48 measurements in the case of Kr and 94 in the case of Xe.

IV. THEORETICAL RESULTS

This section briefly describes the TDCIS and RRPA theories to which our experimental results will be compared. The TDCIS method is an *ab initio* time-dependent multielectron theory [17,18], which has been applied to Kr and Xe in Refs. [19–21]. Here, we use grid parameters [34] similar to those in Ref. [21]. The XUV and IR fields are represented by Gaussian envelopes of 30-fs duration. Photoelectron spectra are calculated using the splitting method described in Refs. [22,23]. Photoelectron sidebands are calculated for photoemission parallel to the common polarization axis of XUV and IR fields and are integrated over their energy width to obtain the predicted spin-orbit delays.

The RRPA is an *ab initio* time-independent multielectron theory [11,12]. This theory has been used to predict photoionization delays [24,25] and has also been compared to experiments in various rare gases [26–28]. For the present work, we have included the following photoionization channels and all mutual channel interactions: $4p^{-1}$, $4s^{-1}$, and $3d^{-1}$ in the case of Kr and $5p^{-1}$, $5s^{-1}$, $4d^{-1}$, and $4p^{-1}$ in the case of Xe. In both cases all fine-structure components of all channels were included. In what follows, we use the atomic units unless otherwise specified. Within the dipole approximation, the photoionization amplitudes contributing to photoemission along the polarization direction of the ionizing radiation are given by [29]

$$\begin{aligned} T^{m=1/2}_{np_{1/2}} &= \frac{1}{\sqrt{6}} Y_{00} D_{np_{1/2}\to\epsilon s_{1/2}} + \frac{1}{\sqrt{15}} Y_{20} D_{np_{1/2}\to\epsilon d_{3/2}}, \\ T^{m=1/2}_{np_{3/2}} &= \frac{1}{\sqrt{6}} Y_{00} D_{np_{3/2}\to\epsilon s_{1/2}} - \frac{1}{5\sqrt{6}} Y_{20} D_{np_{3/2}\to\epsilon d_{3/2}} \\ &\quad - \frac{1}{5}\sqrt{\frac{3}{2}} Y_{20} D_{np_{3/2}\to\epsilon d_{5/2}}, \end{aligned} \tag{1}$$

where $Y_{\ell m}$ represent the values of the spherical harmonics $Y_{\ell m}(\theta = 0, \phi = 0)$ and $D_{np_j\to\epsilon\ell'_{j'}}$ are the reduced photoionization matrix elements defined in Refs. [11,35]. Since our measurements are integrated over the emission direction of the photoelectron by virtue of the magnetic-bottle configuration, possible effects of this angular averaging on the observed delays must be considered. We have therefore calculated the delays for different emission angles using the complete off-axial expressions given in Ref. [29]. In the case of Kr, the spin-orbit delays vary with angle by less than 5 as and the variation is even smaller in the case of Xe. We therefore neglected the angle dependence in our further analysis and compare our measurements with calculations carried out for photoemission parallel to the polarization of the XUV field. The atomic contribution to the delay of a photoelectron wave packet associated with the ^2P_J state of Kr^+ or Xe^+ is calculated according to

$$\tau_j = \frac{\partial}{\partial E} \arg\left(T_{np_j}\right), \tag{2}$$

which is illustrated in Fig. 3.

The total delay accessible to attosecond interferometry is then obtained by adding the contribution of the continuum-continuum (cc) transition: $\tau^{\rm tot}_j = \tau_j + \tau_{cc,j}$. Several formulas have been given to calculate cc delays (τ_{cc}) based on the phase of the cc transition matrix elements [30]. The simplest approximation, obtained by considering only the long-range phase in the asymptotic part of the wave functions is

$$\phi^{(P)}_{cc}(k,\kappa) \equiv \arg\left(\frac{(2\kappa)^{iZ/\kappa}}{(2k)^{iZ/k}} \frac{\Gamma[2 + iZ(1/\kappa - 1/k)]}{(\kappa - k)^{iZ(1/\kappa - 1/k)}}\right), \tag{3}$$

where k and κ are the photoelectron momenta before and after interaction with the IR field, respectively. These continuum-continuum delays are displayed in Fig. 4.

The next better approximation consists in correcting Eq. (3) for the long-range variation of the amplitudes of the scattering wave functions:

$$\phi^{(PA)}_{cc}(k,\kappa) \equiv \phi^{(P)}_{cc}(k,\kappa) + \alpha(k,\kappa), \tag{4}$$

where

$$\alpha(k,\kappa) = \arg\left[1 + \frac{iZ}{2}\left(\frac{1}{\kappa^2} + \frac{1}{k^2}\right)\frac{\kappa - k}{1 + iZ(1/\kappa - 1/k)}\right]. \tag{5}$$

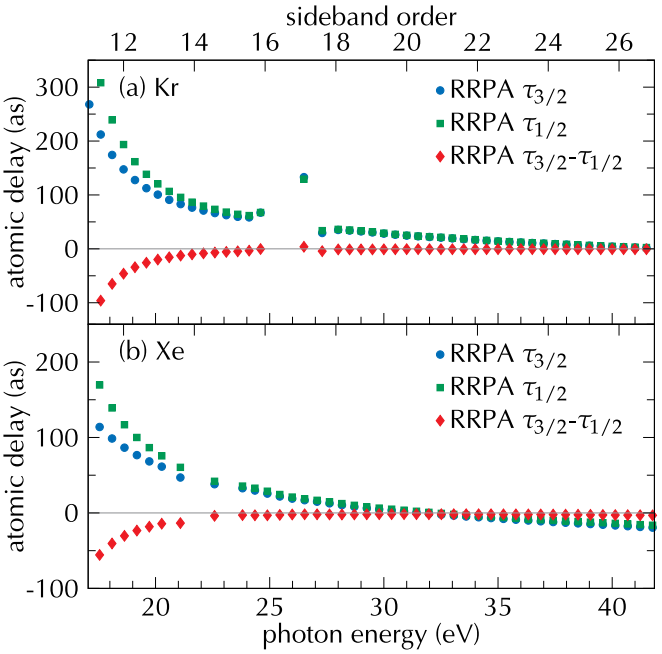

FIG. 3. Atomic delays ($\tau_{3/2}$ and $\tau_{1/2}$) between photoelectrons associated with the $^2P_{3/2}$ and $^2P_{1/2}$ final states of (a) Kr^+ and (b) Xe^+ obtained from the RRPA calculations.

A further improvement of the cc delays was obtained by regularizing the wave functions at the origin by substituting the radial coordinate with a complex variable. This approach provides quasiexact results in the case of atomic hydrogen, as can be judged from the comparison with exact numerical calculations [30].

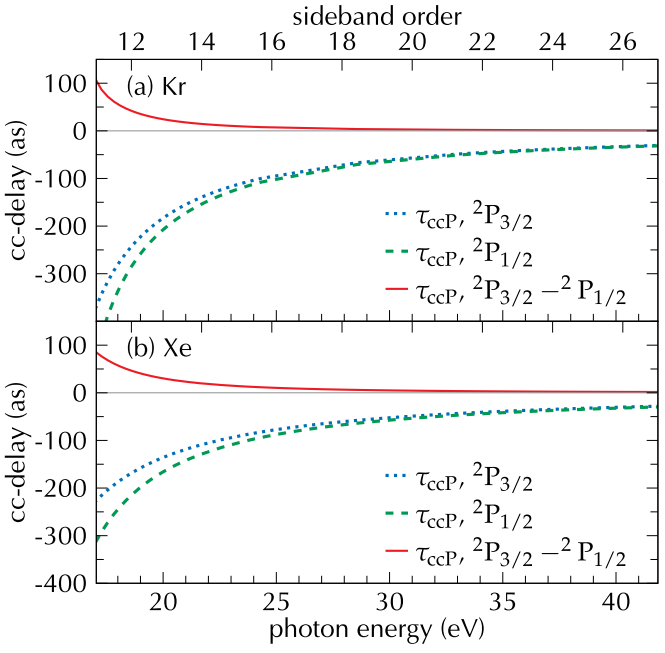

FIG. 4. Continuum-continuum delays ($\tau_{ccP,3/2}$, $\tau_{ccP,1/2}$), and their difference, pertaining to photoelectron wave packets associated with the $^2P_{3/2}$ and $^2P_{1/2}$ final states of (a) Kr^+ and (b) Xe^+ obtained from Eq. (3).

V. DISCUSSION

We now compare the results of the experiment with the TDCIS and RRPA results in Fig. 2. In the case of krypton, quantitative agreement is obtained between experiment and the RRPA theory for most of the data points, when we use Eq. (3) to evaluate the cc delays. The missing points between 25 and 29 eV are a consequence of the presence of singly excited resonances converging to the $4s^{-1}$ threshold of Kr at 27.51 eV. This region was partially left out of the RRPA calculation because the spin-orbit delays display very large variations in the vicinity of the resonances. We have, however, very carefully studied the possible influence of these autoionizing resonances on the measured delays in our experiment. We have systematically varied the central wavelength of the Ti:Sa laser system and have used emission lines from a discharge-generated plasma source to calibrate the XUV-photon spectrometer. Although we have observed clear shifts of the high-harmonic photon energies, sufficient to fulfill the resonance conditions with singly excited states, no systematic dependence of the measured photoionization delays on the photon energies could be determined. Therefore, all measurements were averaged together, yielding the data points shown in Fig. 2(a). This is an interesting observation, because the effects of resonances on the phase of photoelectron side-band oscillations [31] and electronic photoionization delays [32] have been observed and reproduced by theory in the case of other atomic systems.

The experimental results in Fig. 2(a) also agree well with the TDCIS calculations. The calculated delays lie within the 95% confidence intervals of our measurements for all energies that are not affected by autoionizing resonances. The data points between 24.8 eV (SB16) and 31.0 eV (SB20) agree with the TDCIS delays within two times the 95% confidence intervals. The possible effects of the singly excited resonances were further investigated by comparing the results of TDCIS calculations in which only the $4p^{-1}$ channel was active, with calculations in which both the $4p^{-1}$ and the $4s^{-1}$ channels were active and interchannel coupling was included. The difference between the two calculations was systematically smaller than 3 as, confirming our experimental conclusion to the insignificant influence of the singly excited autoionizing resonances on the spin-orbit delays.

In the case of xenon [Fig. 2(b)], significant discrepancies are found between experiment and theory. Although the first and third data points agree with the RRPA calculations combined with Eq. (3), the three other data points lie far away from the theoretical results. The region between 20.5 and 23.5 eV is affected by autoionizing resonances in the vicinity of the $5s^{-1}$ threshold of Xe^+ at 21.77 eV and is therefore left out of the RRPA calculations. As in the case of Kr, we have systematically investigated the possible influence of the singly excited resonances converging to the $5s^{-1}$ threshold of Xe^+ at 23.40 eV, on the delay measured at 21.7 eV (SB14) but have not found any systematic effect. The delays calculated by the TDCIS method in Fig. 2(b) are closer to zero than the RRPA results at low energies, but agree well with the RRPA results at higher energies. As in the case of Kr, TDCIS calculations including only the $5p^{-1}$ channel or both the $5p^{-1}$ and the $5s^{-1}$ channel differ by less than 4 as.

What are possible origins for the large discrepancy between experiment and theory in the case of xenon? First, although RRPA and TDCIS fully include the singly excited states, such as the autoionizing resonances converging to the $5s^{-1}$ threshold (full green lines in Fig. 2), neither RRPA nor TDCIS include doubly excited states, i.e., states that are dominated by two-electron-two-hole configurations (gray lines in Fig. 2). The interaction between singly and doubly excited states is entirely mediated by electron correlation, which makes such effects very interesting from a fundamental point of view. The absence of doubly excited states from RRPA has indeed been identified as the dominant origin of inaccuracies in the calculation of photoelectron-asymmetry parameters in argon [33]. The high density of doubly excited states in the region of 26–33 eV in Xe is therefore a likely explanation for the observed deviations between experiment and theory (both TDCIS and RRPA). In other words, the incomplete treatment of electron correlation in both RRPA and TDCIS, is the most likely explanation for the observed discrepancy. In further support of this conclusion, we note that in the region above ∼25 eV, the contribution of the continuum-continuum delays is negligible (<10 as in Xe and <8 as in Kr; Fig. 3), which enables us to attribute the observed deviations to the atomic part τ_j of the photoionization delays.

Second, the treatment of spin-orbit coupling in TDCIS is approximate. Although spin-orbit coupling is fully included in the angular-momentum algebra underlying the TDCIS code, the radial electronic wave functions are the same for both spin-orbit channels. Relativistic effects are, however, expected to affect the radial wave functions of these two channels differently with the largest differences expected for low kinetic energies. This fact is likely to explain why the spin-orbit delays are underestimated in the TDCIS calculation of the lowest two photon energies in Xe (see Fig. 2), whereas they agree well with the RRPA calculations at the highest three photon energies.

Third, a possible reason for the deviation between experiment and theory at 27.9 and 31.0 eV is the sensitivity of spin-orbit delays to the phase shifts between continuum channels associated with the $^2P_{3/2}$ state on one hand and the $^2P_{1/2}$ state on the other. These phase shifts play little or no role in any traditional observable of photoelectron spectroscopy, such as cross sections, angular distributions or spin-polarization parameters [8,9]. Measurements of photoionization delays between photoelectrons leaving the ion in one of the two spin-orbit states are, however, mainly sensitive to these phase shifts. Therefore, it is conceivable that both theories are not sufficiently accurate in predicting these phase shifts.

Since our measurements probe delays between photoelectrons associated with close-lying ionization thresholds at low kinetic energies they additionally offer the possibility of testing the performance of several analytical expressions for the hydrogenic continuum-continuum delays in the case of heavier atoms. The atomic part of the relative delays $\tau_{3/2}$ and $\tau_{1/2}$, with τ_j given by Eq. (2) and shown in Fig. 3, increase to large positive values towards the ionization threshold because they are dominated by the contribution of the Coulomb potential. The difference $\tau_{3/2} - \tau_{1/2}$ decreases to large negative values because the $^2P_{3/2}$ ionization threshold lies below the $^2P_{1/2}$ threshold. The large negative relative atomic delays $\tau_{3/2} - \tau_{1/2}$ are compensated by large positive differences of the cc delays at low kinetic energies (Fig. 4). Therefore, the total relative delays at low kinetic energies must be very sensitive to each of the two contributions.

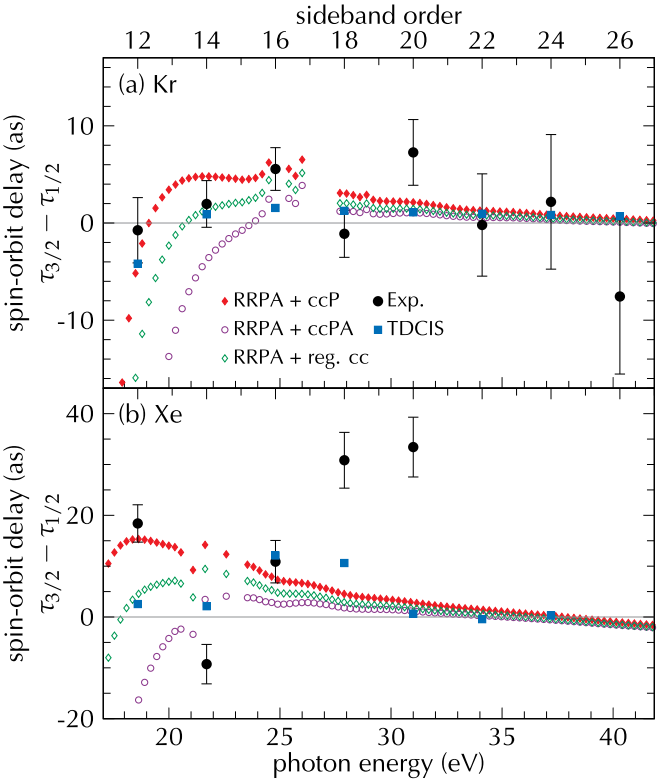

FIG. 5. Comparison of the measured delays ($\tau_{3/2} - \tau_{1/2}$) with RRPA calculations combined with different versions of the continuum-continuum delays. The version "ccP" refers to Eq. (3), "ccPA" refers to Eq. (4), and "reg" refers to the cc delays calculated on the basis of the regularized radial wave functions (see text and Ref. [30] for details).

Figure 5 compares the experimental measurements and TDCIS results to the sum of the atomic delay from RRPA calculations and the analytical cc delays. The largest effects are seen at low photon energies, as expected. In the cases of both Kr and Xe, the cc delays calculated according to Eqs. (3) and (5) yield the best results. Using Eq. (4) markedly deteriorates the agreement with the lowest experimental points. In the case of Kr, the agreement between the results of Eqs. (3) and (5) is quantitative with most of the experimental data points, as well as with the TDCIS results. A similar situation occurs in xenon. The data points at 18.6 and 24.8 eV agree best with the predictions of Eq. (3), followed by Eq. (5), and finally by Eq. (4), for which the worst agreement with experiment is obtained. Concerning the data point at 21.7 eV, we recall the proximity of multiple doubly excited states, such that one cannot expect quantitative agreement for this data point.

VI. CONCLUSIONS

In conclusion, we have realized precision measurements of delays between photoelectron wave packets associated with the spin-orbit components of the electronic ground states

of Kr^+ and Xe^+. In the case of krypton, the spin-orbit delays were found to be small, amounting to less than 8 attoseconds in the investigated range of photon energies. This result quantitatively agrees with state-of-the-art theories. In the case of xenon, much larger spin-orbit delays were measured, reaching up to 33 ± 6 as at a photon energy of 33.4 eV. These results demonstrate the importance of fine-structure effects, such as spin-orbit coupling, in photoemission time delays. This is particularly important for photoemission from all samples in the gas or condensed phases containing heavy elements [3–5]. Even more importantly, our results suggest significant shortcomings in state-of-the-art theories of atomic photoionization which were known to achieve near-quantitative accuracy in traditional photoemission experiments. The most likely explanation of this deficiency is an incomplete treatment of electron correlation, arising from the absence of doubly excited configurations in TDCIS and RRPA. Our work therefore contributes to demonstrate that attosecond metrology has now reached the level to challenge well-established theories and therefore has the potential for driving major progress in our understanding of electron correlation in multielectron systems.

ACKNOWLEDGMENTS

We thank U. Keller and her group for discussions. We gratefully acknowledge funding from an ERC Starting Grant (Contract No. 307270-ATTOSCOPE) and the NCCR-MUST, a funding instrument of the Swiss National Science Foundation. S.P. is funded by the Alexander von Humboldt Foundation and by the NSF through a grant to ITAMP. A.S.K. acknowledges support from the Australian Research Council under Discovery Grant No. DP120101805.

I.J. and M.H. contributed equally to this work.

[1] M. Schultze, M. Fiess, N. Karpowicz, J. Gagnon, M. Korbman, M. Hofstetter, S. Neppl, A. L. Cavalieri, Y. Komninos, T. Mercouris *et al.*, Science **328**, 1658 (2010).

[2] K. Klünder, J. M. Dahlström, M. Gisselbrecht, T. Fordell, M. Swoboda, D. Guénot, P. Johnsson, J. Caillat, J. Mauritsson, A. Maquet *et al.*, Phys. Rev. Lett. **106**, 143002 (2011).

[3] A. L. Cavalieri, N. Muller, T. Uphues, V. S. Yakovlev, A. Baltuska, B. Horvath, B. Schmidt, L. Blumel, R. Holzwarth, S. Hendel *et al.*, Nature (London) **449**, 1029 (2007).

[4] R. Locher, L. Castiglioni, M. Lucchini, M. Greif, L. Gallmann, J. Osterwalder, M. Hengsberger, and U. Keller, Optica **2**, 405 (2015).

[5] S. Neppl, R. Ernstorfer, A. L. Cavalieri, C. Lemell, G. Wachter, E. Magerl, E. M. Bothschafter, M. Jobst, M. Hofstetter, U. Kleineberg *et al.*, Nature (London) **517**, 342 (2015).

[6] M. Huppert, I. Jordan, D. Baykusheva, A. von Conta, and H. J. Wörner, Phys. Rev. Lett. **117**, 093001 (2016).

[7] R. Pazourek, S. Nagele, and J. Burgdörfer, Rev. Mod. Phys. **87**, 765 (2015).

[8] N. A. Cherepkov, J. Phys. B **12**, 1279 (1979).

[9] U. Heinzmann, J. Phys. B **13**, 4367 (1980).

[10] C. M. Marian, Wiley Interdisc. Rev.: Computat. Mol. Sci. **2**, 187 (2012).

[11] W. R. Johnson and C. D. Lin, Phys. Rev. A **20**, 964 (1979).

[12] M. Y. Amusia, *Atomic Photoeffect* (Plenum Press, New York, 1990).

[13] J. M. Dahlström, A. L'Huillier, and A. Maquet, J. Phys. B **45**, 183001 (2012).

[14] M. Huppert, I. Jordan, and H. J. Wörner, Rev. Sci. Instrum. **86**, 123106 (2015).

[15] I. Jordan, M. Huppert, M. A. Brown, J. A. van Bokhoven, and H. J. Wörner, Rev. Sci. Instrum. **86**, 123905 (2015).

[16] K. Codling and R. P. Madden, J. Res. Nat. Bur. Stand. **76A**, 1 (1972).

[17] L. Greenman, P. J. Ho, S. Pabst, E. Kamarchik, D. A. Mazziotti, and R. Santra, Phys. Rev. A **82**, 023406 (2010).

[18] S. Pabst and R. Santra, Phys. Rev. Lett. **111**, 233005 (2013).

[19] E. Goulielmakis, Z.-H. Loh, A. Wirth, R. Santra, N. Rohringer, V. S. Yakovlev, S. Zherebtsov, T. Pfeifer, A. M. Azzeer, M. F. Kling *et al.*, Nature (London) **466**, 739 (2010).

[20] S. Pabst, A. Sytcheva, A. Moulet, A. Wirth, E. Goulielmakis, and R. Santra, Phys. Rev. A **86**, 063411 (2012).

[21] S. Pabst, M. Lein, and H. J. Wörner, Phys. Rev. A **93**, 023412 (2016).

[22] X. M. Tong, K. Hino, and N. Toshima, Phys. Rev. A **74**, 031405 (2006).

[23] A. Karamatskou, S. Pabst, Y.-J. Chen, and R. Santra, Phys. Rev. A **89**, 033415 (2014).

[24] A. S. Kheifets and I. A. Ivanov, Phys. Rev. Lett. **105**, 233002 (2010).

[25] A. S. Kheifets, Phys. Rev. A **87**, 063404 (2013).

[26] D. Guénot, K. Klünder, C. L. Arnold, D. Kroon, J. M. Dahlström, M. Miranda, T. Fordell, M. Gisselbrecht, P. Johnsson, J. Mauritsson *et al.*, Phys. Rev. A **85**, 053424 (2012).

[27] D. Guénot, D. Kroon, E. Balogh, E. W. Larsen, M. Kotur, M. Miranda, T. Fordell, P. Johnsson, J. Mauritsson, M. Gisselbrecht *et al.*, J. Phys. B **47**, 245602 (2014).

[28] C. Palatchi, J. M. Dahlström, A. S. Kheifets, I. A. Ivanov, D. M. Canaday, P. Agostini, and L. F. DiMauro, J. Phys. B **47**, 245003 (2014).

[29] A. S. Kheifets, A. Mandal, P. C. Deshmukh, V. K. Dolmatov, D. A. Keating, and S. T. Manson, Phys. Rev. A **94**, 013423 (2016).

[30] J. Dahlström, D. Guénot, K. Klünder, M. Gisselbrecht, J. Mauritsson, A. L'Huillier, A. Maquet, and R. Taïeb, Chem. Phys. **414**, 53 (2013).

[31] M. Kotur, D. Guénot, Á. Jiménez-Galán, D. Kroon, E. W. Larsen, M. Louisy, S. Bengtsson, M. Miranda, J. Mauritsson, C. L. Arnold *et al.*, Nat. Commun. **7**, 10566 (2016).

[32] M. Sabbar, S. Heuser, R. Boge, M. Lucchini, T. Carette, E. Lindroth, L. Gallmann, C. Cirelli, and U. Keller, Phys. Rev. Lett. **115**, 133001 (2015).

[33] M. Y. Amusia and A. S. Kheifets, Phys. Lett. A **82**, 407 (1981).

[34] A pseudo-spectral grid with a radial box size of $130a_0$, 600 grid points, and a mapping parameter of $\zeta = 0.5$ are used. The complex absorbing potential starts at $100a_0$ and has a strength of $\eta = 0.002$. The maximum angular momentum is 15 and Hartree-Fock orbitals up to an energy of 10 a.u. are considered. The

propagation method is Runge-Kutta 4 with a time step $dt = 0.05$ a.u. All $5s$ and $5p$ orbitals are active in the calculations on Xe, and similarly all $4s$ and $4p$ orbitals are active in the case of Kr.

[35] We note that the authors of Ref. [29] found the necessity to add an extra parity factor to the expressions of Ref. [11] to make them compatible with the Wigner-Eckhardt theorem.